PERGAMON

International Journal of Heat and Mass Transfer 43 (2000) 2961–2971

International Journal of HEAT and MASS TRANSFER

www.elsevier.com/locate/ijhmt

A parametric study of radiative heat transfer in pulverised coal furnaces

J.G. Marakis*, C. Papapavlou, E. Kakaras

Laboratory of Steam Boilers and Thermal Plants, Thermal Engineering Section, National Technical University of Athens, 28 Octobriou Street, 10682 Athens, Greece

Received 25 June 1999; received in revised form 15 September 1999

Abstract

The P-1 approximation and the Monte Carlo method are applied in cylindrical coal-fired furnaces. The absorption and scattering efficiencies and the phase function of coal, char and fly-ash particles are obtained from Lorenz-Mie theory and wavelength dependent optical properties based on measurements available in the literature. The influence of each kind of particle on the radiative heat transfer is investigated. Comparisons between the P-1 and the Monte Carlo methods are performed for various particle size distributions and mass concentrations. Isotropic and neglecting of scattering are evaluated against anisotropic scattering as potential simplifications in engineering applications.

Keywords: Furnaces; Monte Carlo; Radiation

1. Introduction

Thermal radiation is the dominant heat transfer mode in pulverised coal-fired furnaces [1]. A factor that significantly complicates the analysis in these furnaces is the presence of coal combustion particles. Coal, char and fly-ash particles absorb, emit and anisotropically scatter thermal radiation. Their radiative characteristics are strongly dependent on their composition, the pulverisation process and the firing system. These parameters affect the optical properties, the particle size distributions and the mass concentrations, respectively, which in turn affect the extinction coefficient, the scattering albedo and the angular distribution of the scattered intensity of the particulate phase. The overall contribution of this phase to radiative heat transfer in coal-fired furnaces increases proportionally to the particle loading. Therefore, even being significant in atmospheric coal combustion, particulate radiation is expected to be a key design parameter for novel coal utilisation technologies, characterised by increased particle loading, such as the Pressurised Pulverised Coal Combustion (PPCC).

The objective of the present study is to evaluate some of the methods, models and assumptions that are used for the prediction of the radiant exchange in coal-fired furnaces. These methodological approaches can be distinguished in two categories;

Abbreviations: MC, Monte Carlo; PPCC, Pressurised Pulverised Coal Combustion; psd, particle size distribution; RTE, Radiative Transfer Equation.

* Corresponding author. Lehrstuhl für Strömungsmechanik, Universität Erlangen-Nürnberg, Cauerstraße 4, D-91058 Erlangen, Germany.

E-mail address: jmarakis@lstm.uni-erlangen.de (J.G. Marakis).

0017-9310/00/$ - see front matter
PII: S0017-9310(99)00347-6

Nomenclature

a	parameter in Eq. (9)
A	projected area of particles per unit mass
b	parameter in Eq. (6)
c	parameter in Eq. (9)
D	diameter
f_v	volume fraction
g	asymmetry factor
I	radiative intensity
I_0	zeroth order moment of the radiative intensity
I_i	ith order moment of the radiative intensity
k	imaginary part of m
l_i	direction cosines
m	complex refractive index
n	real part of m
p	phase function
Q	efficiency
q_w	wall flux
Q_w	total wall flux
r, φ, z	cylindrical co-ordinates
R	random variable
s	distance
t	parameter in Eq. (6)
T	temperature
W	mass concentration
x	particle size parameter

Greek symbols

β	parameter in Eq. (6)
δ	Kronecker's delta
ε	emissivity
ϑ	polar angle
κ	absorption, extinction, scattering coefficient
λ	wavelength
ξ, η, ζ	direction cosines
ρ	reflectivity
τ	optical thickness
φ	azimuth angle
ψ	scattering angle
ω	scattering albedo
Ω	solid angle

Subscripts

20	quadratic mean diameter
32	Sauter mean diameter
a	absorption
b	black body
c	coal
ch	char
e	extinction
f	fly-ash
m	most probable
r	radial
s	scattering, soot
w	wall
λ	spectral
ρ	reflectivity

Superscripts

$'$	before scattering
–	psd averaged
$*$	Planck averaged

first, methods for the solution of the radiant exchange and second, methods for the calculation of the radiative properties. In this study, for assessments in the first category, reference results will be provided by a Monte Carlo (MC) method. The applications of this method in various fields of thermal engineering have been recently reviewed by Howell [2]. In the area of furnace modelling, (MC) method have been applied in Refs. [3–7]. Although the method has many well-known advantages, such as exactness for sufficiently large statistical samples and flexible incorporation of detailed physical submodels, it also has the disadvantage that it requires long execution times. This disadvantage is crucial for furnace modelling, because the strong coupling of radiation with the flow field and the chemical reactions implies an iterative solution of the energy equation. In this case, an approximate method is usually adopted for the fast computation of the radiative source term occurring in the energy equation. Methods belonging to this category are the P–N approximations [8–13]. These methods use expansions of the local intensity in terms of spherical harmonics, with truncation to N terms in the series and substitution into the moments of the differential form of the Radiative Transfer Equation (RTE). In the present study, the lowest order P-1 approximation is evaluated.

Equally important to the solution methods are the models used for the prediction of the radiative properties of the coal combustion particles [1,14]. Coal and char strongly extinguish thermal radiation, however, their presence is restricted in the near burner area of a furnace. In contrast, fly-ash may be found in larger volumes including the heat recovery section of a furnace. Many studies, including Gupta et al. [5], Blokh [15], Boothroyd and Jones [16] and references cited therein, indicated that fly-ash is an important — perhaps dominating — contributor to radiative transfer in pulverised coal furnaces. Good-

win and Mitchner [17] published measurements of the wavelength dependent real and imaginary parts of fly-ash refractive index. Apart from the strong wavelength dependence, these measurements showed significantly lower values for the imaginary part of the fly-ash refractive index. Goodwin's measurements have been discussed by Im and Ahluwalia [18], who proposed dispersion formulas dependent on ash chemical composition and by Liu and Swithenbank [19], who investigated the influence of the particle size distribution on the fly-ash radiative properties. The present study attempts to quantify the effect of these fly-ash optical properties on the overall heat transfer inside a furnace.

For that purpose, an algorithm is needed to connect the optical properties of single particles with the extinction coefficient, scattering albedo and angular distribution of the scattered intensity of particle clouds. The first step of this algorithm, based on the assumption of spherical homogeneous particles and the measured wavelength dependent optical properties, will estimate the extinction and scattering efficiencies of single particles using the Lorenz–Mie theory (Bohren and Huffman [20]). The applicability of this approach for a cloud of fly-ash particles suspended in a small fluidised bed has been verified by Boothroyd et al. [21]. The second step of the algorithm extends the single particle properties to the particle cloud properties encountered in the RTE. For this step, the local concentrations and size distributions have to be determined. The underlying assumption in this algorithmic step is the single scattering per control volume. In general, this assumption can be valid by appropriately adjusting the size of each control volume. Especially for the Monte Carlo method, an *ad hoc* estimation of the validity of this assumption is possible, with small computational overhead, by keeping for each control volume, an account of the ratio of the multiple to the total scatterings.

In the following paragraphs, the methods for the calculation of the radiant exchange and the radiative properties of the combustion products inside a coal-fired furnace are described. The emphasis is placed on the real properties of the coal combustion particles and their effects on the overall heat transfer. Results are presented for two-dimensional cylindrical furnaces. Test cases showing the influence of each kind of particles and the assumptions related to their scattering behaviour are presented for different particle concentrations and particle size distributions. The test cases are solved with both the accurate Monte Carlo and the approximate P-1 methods. Concluding remarks on the applicability and effectiveness of the examined modelling approaches are discussed in the last paragraphs.

2. Formulation

For an absorbing, emitting and scattering mixture of coal combustion gases and particles in local thermodynamic equilibrium which is enclosed in a two-dimensional axisymmetric cylindrical furnace, the spectral RTE is written (Mengüç and Viskanta [10])

$$\left[\frac{1}{\kappa_{\lambda,\,\mathrm{e}}}\left(\xi\frac{\partial}{\partial r}-\frac{n}{r}\frac{\partial}{\partial\varphi}+\zeta\frac{\partial}{\partial z}\right)+1\right]I_\lambda(\vec{r},\Omega) = (1-\omega_\lambda)I_{\mathrm{b},\,\lambda}(T(\vec{r})) + \frac{\omega_\lambda}{4\pi}\int_{4\pi} I_\lambda(\vec{r},\Omega')p_\lambda(\Omega,\Omega')\,\mathrm{d}\Omega' \quad (1)$$

where $\xi=\sin\vartheta\cos\varphi$, $\eta=\sin\vartheta\sin\varphi$, $\zeta=\cos\vartheta$ are the direction cosines, φ and ϑ are the azimuth and polar angles, $\kappa_{\lambda,\,\mathrm{e}}$ the spectral extinction coefficient, ω_λ the single scattering albedo and $p_\lambda(\Omega,\Omega')$ the phase function of the medium.

For the solution of Eq. (1) in coal-fired furnaces, a method is required to determine the field distributions of the absorption and scattering coefficients and the phase function of the medium. Since the present study focuses on particulate radiation, the flue gases will be simply characterised by a prescribed absorption coefficient leaving the investigation of their detailed spectral modelling for a separate publication (Marakis [22]). The particulate phase may consist of coal, char, fly-ash and soot particles. The latter will be considered as absorbing, emitting and non-scattering agents. In general, a simplified treatment of soot radiation in coal-fired furnaces is justified by the uncertainties related with soot formation under coal-volatile combustion.

The extinction coefficient of a particle cloud following a size distribution $f(D)$, where D is the particle diameter, is associated with the averaged extinction efficiency $\bar{Q}_{\lambda,\,\mathrm{e},\,i}$ through the following equation (Goodwin and Mitchner [17])

$$\bar{\kappa}_{\lambda,\,\mathrm{e},\,i}=W_iA_i\bar{Q}_{\lambda,\,\mathrm{e},\,i} \quad (2)$$

where i denotes either coal, char or fly-ash, W_i is the mass concentration of the ith kind of particles (kg m^{-3}), $A_i=3(2\rho_iD_{32,\,i})^{-1}$ is the projected area of the particles per unit mass (m^2 kg^{-1}) and ρ_i the density of the ith kind of particles (kg m^{-3}). The scattering coefficient $\kappa_{\lambda,\,\mathrm{s},i}$ of a particle cloud is determined by an equation similar to (2). Dropping the i subscript for convenience, the averaged, over the particle distribution, efficiencies are estimated from the efficiencies of each particle diameter as

$$\bar{Q}_{\lambda,\,\mathrm{e}} = \frac{\int_0^\infty D^2 Q_{\lambda,\,\mathrm{e}}(D) f(D)\,\mathrm{d}D}{D_{20}^2} \tag{3}$$

The characteristic diameters D_{20} and D_{32} are the quadratic and Sauter mean diameters of the particle size distribution $f(D)$ defined by the following equations

$$D_{20}^2 = \int_0^\infty D^2 f(D)\,\mathrm{d}D \tag{4}$$

$$D_{32} = \int_0^\infty D^3 f(D)\,\mathrm{d}D \Big/ \int_0^\infty D^2 f(D)\,\mathrm{d}D \tag{5}$$

A general expression for the particle size distribution, from which simpler forms used in various engineering fields can be derived, is the gamma particle size distribution (psd) discussed in Blokh [15]

$$f(D) = \frac{t b^{(\beta+1)/t} D^\beta \mathrm{e}^{-\beta D/D_\mathrm{m}}}{\Gamma((\beta+1)/t)} \tag{6}$$

where $\Gamma(x)$ denotes the gamma function of the variable x, $b = (\beta/t) D_\mathrm{m}^{-t}$, D_m is the most probable diameter and β, t are adjustable parameters. Furthermore, the psd-averaged asymmetry factor is estimated as

$$\bar{g}_\lambda = \frac{\int_0^\infty Q_{\lambda,\,\mathrm{s}}(D) f(D) D^2 g_\lambda(D)\,\mathrm{d}D}{\int_0^\infty Q_{\lambda,\,\mathrm{s}}(D) f(D) D^2\,\mathrm{d}D} \tag{7}$$

where $g_\lambda(D)$ is the particle asymmetry factor defined as the averaged, over the solid angle, value of the particle phase function

$$g_\lambda(D) = \frac{1}{4\pi} \int_{4\pi} p_\lambda(m, x, \Omega) \cos\vartheta\,\mathrm{d}\Omega \tag{8}$$

In Eq. (8), $m = n + ik$ is the complex refractive index of the medium and $x = \pi D/\lambda$ is the size parameter. The optical properties n and k are wavelength dependent. Table 1 summarises the formulas used in the present study to account for this dependence. For coal and char particles, optical properties are based on the measurements of Brewster and Kunitomo [23]. This set of measurements has been discussed by Im and Ahluwalia [18] and Solomon et al. [24]. It covers the wavelength region $2 < \lambda < 20$ μm. For wavelengths $0.5 < \lambda < 2$ μm, due to the absence of a better approximation, the optical properties are linearly extrapolated from the previous region. For the real part of the fly-ash refractive index, there is essential agreement in the literature for the values included in Table 1 (see also Refs. [5,15,16,21]). In contrast, the imaginary part, as measured by Goodwin [17], differs significantly from previous estimations, exhibiting a strong wave-

Table 1
Wavelength dependent optical properties of coal combustion particles

Particle	Reference	Optical property		Range
Coal	Brewster and Kunitomo [23], Fig. 4	n_λ	Data points	$2 < \lambda < 20$
	Brewster and Kunitomo [23], Fig. 5	k_λ	$2.4 \times 10^{-3(\lambda-2)}$	$2 < \lambda < 20$
Char	Brewster and Kunitomo [23], Fig. 7	n_λ	$1.9 + 9.7 \times 10^{-2(\lambda-2)}$	$2 < \lambda < 5$
			$2.1 + 7.7 \times 10^{-2(\lambda-5)}$	$5 < \lambda < 12$
	Brewster and Kunitomo [23], Fig. 7	k_λ	$2.3 + 1.3 \times 10^{-(\lambda-2)}$	$2 < \lambda < 5$
			$2.7 + 6.1 \times 10^{-2(\lambda-5)}$	$5 < \lambda < 12$
Fly ash	Goodwin and Mitchner [17], Fig. 1(b)	n_λ	1.5	$0.5 < \lambda < 6$
	Liu and Swithenbank [19]		$1.5 - 0.4(\lambda - 6)$	$6 < \lambda < 8$
			$0.8 + 0.5(\lambda - 8)$	$8 < \lambda < 11$
			$2.3 - 0.5(\lambda - 11)$	$11 < \lambda < 12$
	Goodwin and Mitchner [17], Fig. 1(b)	$k_{\lambda,\,T=300\ \mathrm{K}}$	$10^{-4.6+2.2(\lambda-0.5)}$	$0.5 < \lambda < 1$
	Liu and Swithenbank [19]		$10^{-3.5}$	$1 < \lambda < 4$
			$10^{-3.5+(\lambda-4)}$	$4 < \lambda < 5$
			$10^{-2.5+0.2(\lambda-5)}$	$5 < \lambda < 7.5$
			$10^{-1.9+1.8(\lambda-7.5)}$	$7.5 < \lambda < 8.5$
			$10^{-0.1}$	$8.5 < \lambda < 10.5$
			$10^{-0.1-0.7(\lambda-10.5)}$	$10.5 < \lambda < 12$
	Goodwin and Mitchner [17], Fig. 1(b)	$k_{\lambda,\,T=1080\ \mathrm{K}}$	$k_{\lambda,\,T=300\ \mathrm{K}}$	$0.5 < \lambda < 5$
			$10^{-2.5+0.3(\lambda-5)}$	$5 < \lambda < 5.5$
			$10^{-2.2+0.4(\lambda-5.5)}$	$5.5 < \lambda < 7.8$
			$10^{-1.4+1.8(\lambda-7.8)}$	$7.8 < \lambda < 8.5$
			$k_{\lambda,\,T=300\ \mathrm{K}}$	$8.5 < \lambda < 12$

length dependence and generally lower values. The effect of this substantially lower imaginary part on the overall radiative heat transfer in a coal-fired furnace will be examined in Section 3.

The formulas of Table 1 are used to provide the complex refractive index of coal, char and fly-ash as input to the BHMIE program ([20]). The output of this program are the particle extinction and scattering efficiencies $Q_{\lambda,\,e}(D)$, $Q_{\lambda,\,s}(D)$ and the asymmetry factor $g_\lambda(D)$, which are then introduced into Eqs. (3) and (7), respectively, to estimate the psd-averaged extinction coefficient $\bar{\kappa}_{\lambda,\,e}$, scattering coefficient $\bar{\kappa}_{\lambda,\,s}$ and the asymmetry factor $\bar{g}_\lambda$. A further averaging over the black body intensity distribution function allows the determination of the Planck-mean properties $\bar{\kappa}_e^*$, $\bar{\kappa}_s^*$ and $\bar{g}^*$ ([5]).

The highly forward scattering behaviour of the coal combustion particles is satisfactorily represented by the delta-Eddington phase function ([25], also used in Refs. [5,10,14])

$$p(\Omega, \Omega') = 2a\delta(1-\cos\psi) + (1-a)(1+3c\cos\psi) \tag{9}$$

where ψ is the scattering angle: $\cos\psi = \xi\xi' + \eta\eta' + \zeta\zeta'$ and the parameters a and c are related to the coefficients of the Legendre series expansion of the exact phase function [9].

The angular dependence of the radiative intensity $I_\lambda(\vec{r}, \Omega)$ may be expressed by a series of spherical harmonics. In the P-1 approximation, the retention of the first four terms results in transformation of Eq. (1) into the following equation (see [9,10] for details on this derivation)

$$\frac{\vartheta}{\vartheta r}\left(\frac{1}{\bar{\kappa}^*}\frac{\vartheta I_0}{\vartheta r}\right) + \frac{1}{r\bar{\kappa}^*}\frac{\vartheta I_0}{\vartheta r} + \frac{\vartheta}{\vartheta z}\left(\frac{1}{\bar{\kappa}^*}\frac{\vartheta I_0}{\vartheta z}\right) = -3\bar{\kappa}_a^*(4\pi I_b - I_0) \tag{10}$$

Eq. (10) contains only spectrally averaged quantities. Specifically, $\bar{\kappa}^* = \bar{\kappa}_a^* + \bar{\kappa}_s^*(1-\bar{g}^*)$, $\bar{\kappa}_a^* = \bar{\kappa}_e^* - \bar{\kappa}_s^*$ and I_0 is the zeroth moment of $I(\vec{r}, \Omega)$ defined as $I_0 = \int_{4\pi} I(\vec{r}, \Omega)\,\mathrm{d}\Omega$. In the present study, the Marshak boundary condition for diffusely reflecting walls is used together with Eq. (10)

$$I_0 \pm \frac{2(2-\varepsilon_w)}{\varepsilon_w} I_i = 4\pi I_b(T_w) \tag{11}$$

where ε_w is the emissivity at the boundary surfaces, $+$ indicates their positive orientation and I_i is the first order moment of $I(\vec{r}, \Omega)$, defined as $I_i = \int_{4\pi} I(\vec{r}, \Omega) l_i\,\mathrm{d}\Omega$ where l_i denotes one of the direction cosines ξ, η or ζ.

Reference results for the test cases that will be examined in Section 3 will be provided by an MC method. Description of the method and derivation of the probability density functions can be found in textbooks; e.g. Siegel and Howell [26] and Brewster [27]. The random functions used in this study are summarised in Table 2. An explanatory note is needed for the function used to sample the polar angle after a scattering event.

Whenever an energy packet is emitted, a relative system of axes is adapted on it. The z-axis of this system is identical to the propagation direction of the energy packet. In this system, the phase function is symmetric with respect to the azimuth angle. Under this arrangement, when scattering occurs, the polar angle is sampled from the cumulative phase function

$$\int_{-1}^{\xi'} p(\xi)\,\mathrm{d}\xi = 2R_\vartheta \tag{12}$$

In Eq. (12), $p(\Omega, \Omega')$ has been reduced to $p(\xi)$ due to the arrangement of the relative system adapted on the energy packet. The Henyey–Greenstein phase function ([28]) is used in combination with Eq. (12)

$$p(\xi) = \frac{1-\bar{g}^{*2}}{\left(1+\bar{g}^{*2}-2\bar{g}^*\xi\right)^{3/2}} \tag{13}$$

Introduction of Eq. (13) into Eq. (12) yields a closed form expression for sampling the after-scattering polar angles

$$\cos\vartheta = \left(1+\bar{g}^{*2} - \left(\frac{1-\bar{g}^{*2}}{1+2\bar{g}^*R_\vartheta - \bar{g}^*}\right)^2\right)/2\bar{g}^* \tag{14}$$

A set of random variables is used to simulate the stochastic events which, together with the random variables of Table 2, are necessary to complete the Monte

Table 2
Random variables used in the Monte Carlo simulations

Parameter	Phenomenon	Function
φ	Emission from surface and volume, reflection, scattering	$\varphi = 2\pi R_\varphi$
ϑ	Emission from surface, reflection	$\vartheta = \sin^{-1}(\sqrt{R_\vartheta})$
	Emission from volume	$\vartheta = \cos^{-1}(1-2R_\vartheta)$
	Scattering	Eq. (14)
L	Extinction length	$\ln R_L = -\sum_{i=1}^{n} \bar{\kappa}^*_{e,\,tot,\,i,\,s_i}$

Carlo algorithm. This set includes: (i) R_ρ, which is compared to reflectivity to decide whether an energy packet will be absorbed or reflected on a wall boundary, (ii) R_ω, which is compared to the scattering albedo $\bar{\omega}^* = \bar{\kappa}^*_s/\bar{\kappa}^*_e$ to decide whether extinction of an energy packet will be interpreted as absorption or scattering and, (iii) R_g, which is compared to the ratios $\bar{\kappa}^*_{s,\,coal}/\bar{\kappa}^*_{s,\,tot}$ and $(\bar{\kappa}^*_{s,\,coal} + \bar{\kappa}^*_{s,\,char})/\bar{\kappa}^*_{s,\,tot}$ in order to decide whether an energy packet has been scattered on a coal, char or fly-ash particle. After this decision is made, the corresponding value of the asymmetry factor is used in Eq. (14). R_g is introduced because, as will be discussed in the next paragraphs, the coal combustion particles exhibit significantly different behaviour with respect to the angular distribution of the scattered radiative intensity.

3. Results

The methods described in the previous section are applied in a series of test cases with increasing complexity. The approximate P-1 method is evaluated against the reference MC method for a simple test case in Section 3.1, the influence of each kind of coal combustion particles in radiative heat transfer is analysed in Section 3.2 and a sensitivity analysis concerning the effect of particle loading, particle size distribution and simplifications of the scattering pattern is presented in Section 3.3.

3.1. Absorbing and emitting medium

The P-1 approximation is evaluated against the MC method for the simple case, defined in Ref. [29], of an absorbing and emitting medium enclosed in an axisymmetric cylindrical enclosure. The length of the enclosure is 6.29 m and its radius is 1.11 m. The enclosure is subdivided into $i = 1,\ldots,17$ radially homogeneous zones. The temperature distribution is prescribed as $T_i = 2000 - 100(i-1)$, T_i in K. In order to focus on the comparisons between the different methods and modelling approaches, no attempt is made in the present and the following test cases to account for coupling of radiation with the estimation of the temperature field. The wall temperature and emissivity are 300 K and 0.5, respectively. Fig. 1 shows the distributions of the wall heat fluxes calculated by P-1 and MC for two different values of the gas absorption coefficient. For comparison, results from the zonal calculations of Heap et al. [29] are included in this figure. For axial distances greater than 3 m, the fluxes of the zonal method were omitted because they are indistinguishable from those of MC. As it is evident in Fig. 1, for both $\kappa_a = 0.1$ and 0.5 m^{-1}, the zonal and MC methods practically yield the same results. The P-1 approximation predicts satisfactorily accurate radiative wall fluxes in the case of $\kappa_a = 0.5$ m^{-1} (radial optical thickness $\tau_r = 0.555$), while for $\kappa_a = 0.1$ m^{-1} ($\tau_r = 0.111$), differs significantly from both the MC and zonal results.

This inefficiency of the P-1 approximation when applied in optically thin media has been observed by various authors ([8,9]) who agree that P-1 approximation is suitable for modelling the radiative heat transfer in cases where the optical depth is greater than one. Fortunately, as will be shown in the following paragraphs, in pulverised coal fired furnaces, the presence of solid particles results in the increase of the gas-particle mixture extinction coefficient up to levels where the aforementioned limit is satisfied.

3.2. Influence of coal combustion particles

It has been pointed out earlier that a significant body of the relevant literature considers coal, char and fly-ash as main contributors to radiative heat transfer inside pulverised coal-fired furnaces. In order to investigate the influence of each kind of particles a procedure similar to that of Mengüç and Viskanta [14] is followed. These authors considered, as a base case, a furnace containing only flue gases and then they progressively added coal, fly-ash and soot particles. The present study extends this approach by incorporating detailed optical properties of the coal combustion particles and solution of the test cases with both the approximate P-1 and the accurate MC methods.

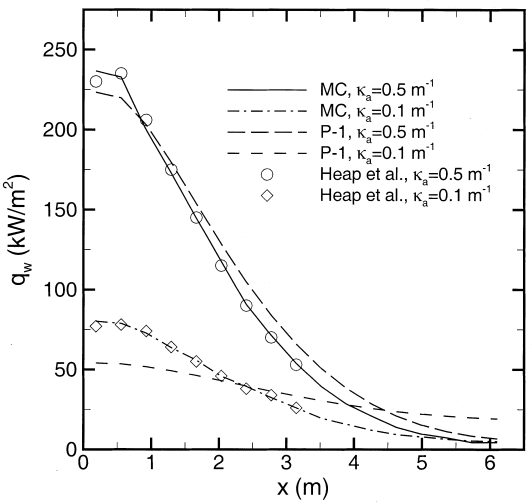

Fig. 1. Comparison of the wall fluxes predicted by the P-1 approximation and the Monte Carlo method for two different absorption coefficients. Symbols correspond to the zonal calculations of Heap et al. [29].

The furnace that will be analysed is shown in Fig. 2. The radiant wall fluxes for this furnace have been measured in Ref. [30] and calculated in Refs. [10,31,32]. Although atmospheric and natural gas-fired, this furnace was found suitable for the sensitivity analysis that will follow because the base case (consideration of only flue gases) has been worked out in the previously mentioned references and also because its high temperature field is representative of the temperature level that is experienced in PPCC combustors. The furnace is divided into three zones. Zone 1 corresponds to the near burner area where considerably large concentrations of coal particles are found. After devolatilisation, coal turns to char, which burns out in zone 2. It is assumed that fly-ash exists everywhere in the furnace, with large concentrations in zones 1 and 2 and small concentration in zone 3. Soot absorption and emission is not included in the test cases of this paragraph. For the analyses of the next paragraph, soot will be assumed to be uniformly distributed inside the furnace with concentration and particle size distribution as indicated in Table 3, and with the spectral absorption coefficient calculated as ([14]) $\kappa_{a,\,soot} = 7f_v/\lambda$, where f_v is the volume fraction. Similar expressions are discussed in [26], while, especially for PPCC conditions, the use of more elaborate approaches does not guarantee improvement of the overall accuracy.

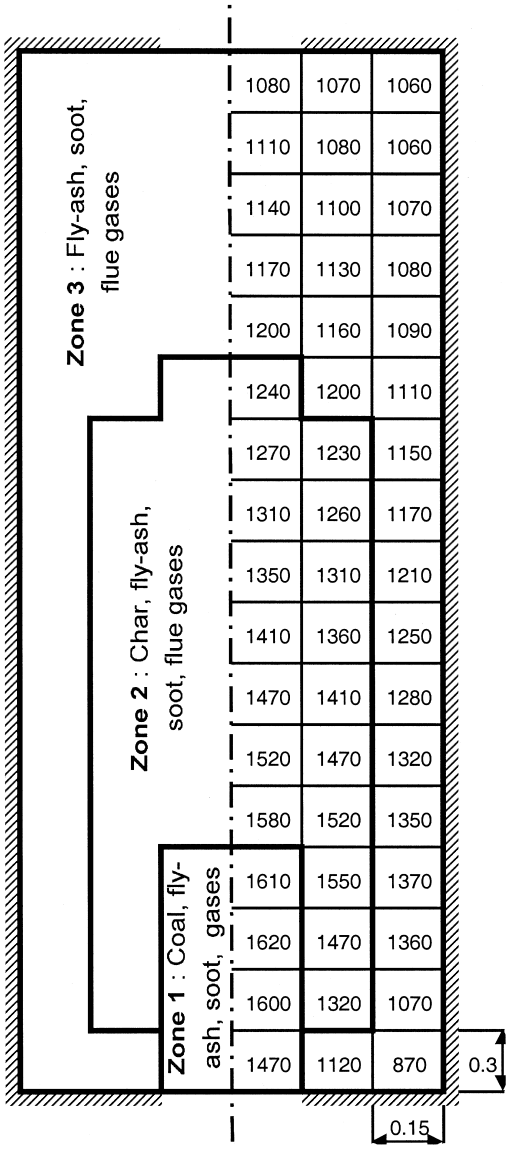

Fig. 2. Furnace geometry, temperature distribution and zoning for the test cases examined in Sections 3.2 and 3.3. The distributions of the particle mass concentrations and sizes are given in Table 3. Other data: wall temperature $T_w = 425$ K, wall emissivity $\varepsilon_w = 0.8$, flue gas absorption coefficient $\kappa_a = 0.3$ m^{-1}.

The size distribution of each kind of particles is represented by a gamma distribution function (Eq. (6)). A simple rule for deriving the most probable diameters of char and fly-ash particles based on the corresponding diameter of the mother coal particle is followed. It should be noted that this rule is used only to facilitate the definition of the test cases examined here and it is not meant to replace other detailed models (see e.g. Ref. [33]) which appropriately account for the evolution of the particle size distributions in coal-fired furnaces due to particle burning and fragmentation. According to this simple rule, the diameter of char shrinks compared to the diameter of coal by a factor of 0.8. Furthermore, it is assumed that the fly-ash concentration in the natural coal is 10% and that six fly-ash particles are produced from each coal particle. The β and t parameters of the gamma distribution function were accepted, for all the cases, as equal to 2. Table 3 summarises the data relevant to the assumed mass concentrations and particle size distributions.

The radiative properties of the coal combustion products are calculated for the mass concentrations corresponding to Case 1 and the 40 μm coal particle diameter. For coal, the Planck-mean absorption coefficient ranges from 3.504 to 3.509 m^{-1}, the scattering coefficient was found from 4.548 to 4.552 m^{-1}, and the asymmetry factor from 0.891 to 0.896. The corresponding values for char were 0.295–0.296 m^{-1} for the absorption coefficient, 0.745–0.746 m^{-1} for the scattering coefficient and 0.674–0.689 for the asymmetry factor. The variation of the fly-ash radiative properties was larger because fly-ash was assumed to be found under two different mass concentrations in zones 1, 2 and 3. The fly-ash absorption coefficient ranged from 0.002 to 0.077 m^{-1}, the scattering coefficient from

Table 3
Data for the test cases examined in Sections 3.2 and 3.3

	Coal	Char	Fly-ash	Soot
Mass concentration (kg/m^3)	2×10^{-1}	2×10^{-2}	2×10^{-2}[a]	1×10^{-4}
Case 1			5×10^{-4}[b]	
Mass concentration (kg/m^3)	5×10^{-1}	1×10^{-1}	5×10^{-2}[a]	1×10^{-4}
Case 2			5×10^{-4}[b]	
Most probable psd[c] diameter (μm)	10	8	3.7	2
Cases 1 and 2	20	16	7.4	2
	30	24	11.1	2
	40	32	14.7	2
	60	48	22.2	2
	80	64	29.4	2

[a] Zones 1 and 2 in Fig. 2.
[b] Zone 3 in Fig. 2.
[c] Eq. (6).

0.026 to 1.093 m^{-1} and the asymmetry factor from 0.727 to 0.762. The lower values of these radiative properties correspond to zone 3 and the higher to zones 1 and 2. Noteworthy is the range of the scattering albedos of these particles. For fly-ash, the scattering albedo it is calculated between 0.93 and 0.95, for coal it is 0.56 and for char it exhibits an intermediate value of 0.71.

The effect of the high fly-ash scattering albedo on the radiative wall flux, as calculated with the MC method, is shown in Fig. 3. Only a slight increase of the wall flux when fly-ash is added to the flue gas is observed. In contrast, when char, which has extinction coefficient in the same order of fly-ash, is added in the mixture, the result is an apparent increase of the wall flux. This is due to the lower scattering albedo of char which allows an absorption coefficient almost an order of magnitude greater than that of fly-ash. Finally, coal alone seems to shape the wall flux near zone 1. Since the optical properties of coal, as shown in Table 1, are on an intermediate level between char and fly-ash, this strong influence is attributed, first, to the high mass concentration of coal in zone 1 and the consequent high absorption coefficient and second, to the quite high transmissivity of zones 2 and 3. It should be noted however that this influence may be overestimated whenever the common modelling assumption that the particulate and gaseous phases are isothermal, is adopted.

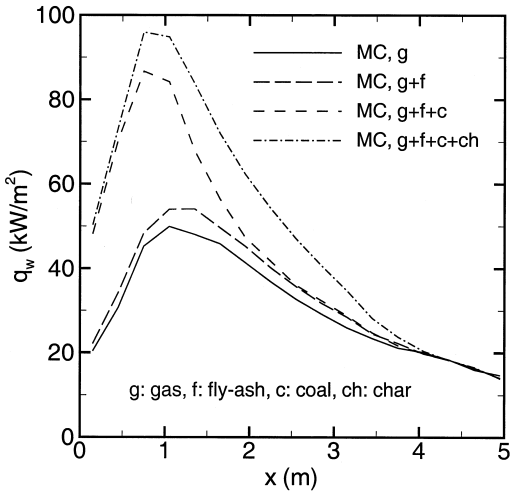

Fig. 3. Effect of coal combustion particles on the distribution of the radiative wall flux as predicted by the Monte Carlo method. Particle mass concentrations as in Table 3, Case 1. Particle size distributions based on the 40 μm coal diameter.

The previous calculations are repeated using P-1 instead of MC. The results, shown in Fig. 4, reveal the same qualitative tendencies as far as the influence of each kind of particle is concerned. In addition, the agreement between P-1 and MC is satisfactory in the cases where coal and char are included in the gas and fly-ash mixture, while the calculated wall flux distributions are apparently different between these two methods when coal and char are ignored. This behaviour is explained by observing that the furnace optical depth is small when only flue gases are considered ($\tau_r = 0.135$), it remains small when fly-ash is added and departs from the optical thin region only when coal and char particles are added. However, even for the latter case, as shown in Fig. 4, especially in the near burner area P-1, compared to MC, tends to smooth the radiative wall fluxes.

3.3. The influence of scattering

The procedure described in the previous paragraph is applied for the mass concentrations denoted as Case

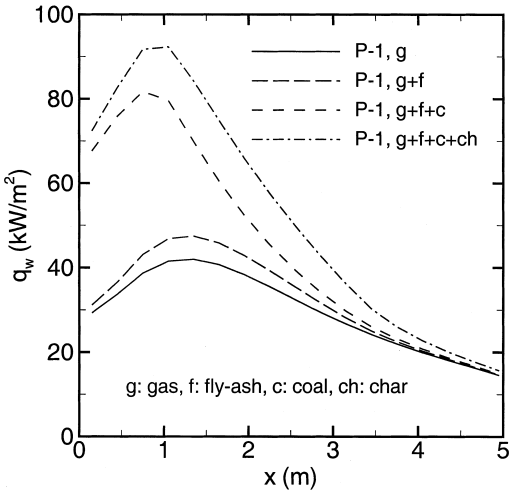

Fig. 4. Same as in Fig. 3, predictions by the P-1 approximation.

1 and Case 2 in Table 3, and for particle size distributions derived from the 10, 20, 30, 40, 60 and 80 μm coal diameter. For each set of diameters and mass concentrations, the calculations were repeated considering anisotropic, isotropic as well as neglecting of scattering. The axial distributions of wall fluxes were then integrated along the peripheral surface to obtain total heat fluxes. These calculations were made with the MC method and were also repeated with the P-1 approximation. Results are presented in Figs. 5 and 6, respectively.

The two methods exhibit similar tendencies. The first phenomenon that is observed in both figures is that scattering enhances absorption. In terms of the MC method, this phenomenon is explained by the enlargement, caused by scattering, of the path length that an energy packet travels inside the furnace. This enlargement increases the possibility of absorption of the energy packet, which in turn results in reduction of the amount of energy packets reaching the wall and consequently, the reduction of wall flux. This enhancement of absorption due to scattering is expected to be more intense in the cases where isotropic scattering is considered, an expectation which is confirmed in the applications of both methods.

The larger discrepancies between the curves corresponding to anisotropic, isotropic and neglecting of scattering occurred for the dense mass concentrations (Case 2), since in these cases, the scattering and absorption coefficients were higher compared to Case 1. In addition, the curves of non-scattering calculations were closer to those of anisotropic scattering, compared to the curves of isotropic scattering. This is explained by the highly forward scattering behaviour of the all kinds of particles, as mentioned in the previous paragraph.

In general, the non-scattering curves lie above the anisotropic scattering ones. However, it is noteworthy that in Fig. 5 and for the dilute concentrations, the points of the non-scattering curve for large diameters lie below the corresponding points of the anisotropic scattering. In MC terms, this phenomenon is explained by the fact that scattering alters the straight-line paths

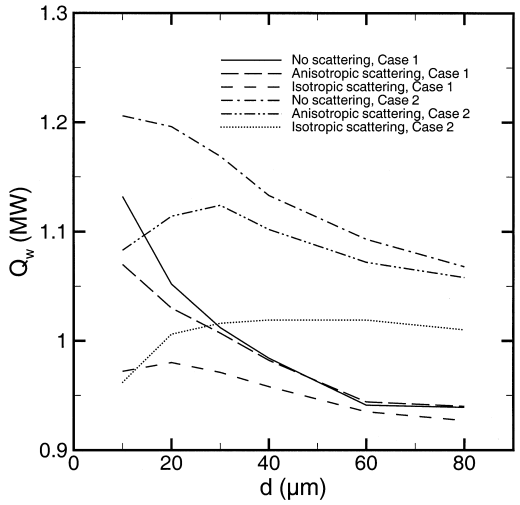

Fig. 5. Effect of the assumption concerning the scattering behaviour of coal combustion particles on the total peripheral wall flux for various particle size distributions as predicted by the Monte Carlo method. Particle mass concentrations and size distributions as in Table 3, Cases 1 and 2.

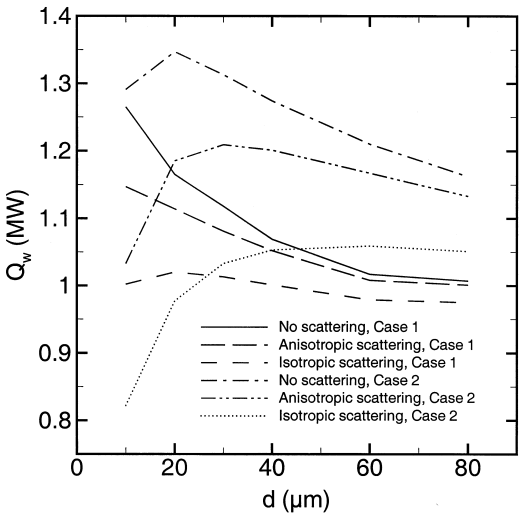

Fig. 6. Same as in Fig. 5, predictions by the P-1 approximation.

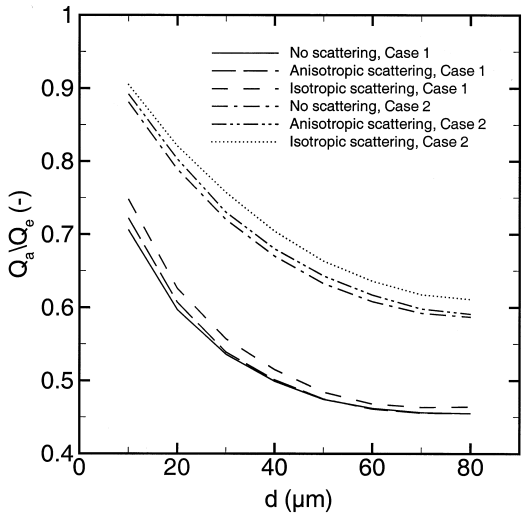

Fig. 7. Enhancement of absorption due to scattering as predicted by the Monte Carlo method assuming isotropic and anisotropic scattering. Particle mass concentrations and size distributions as in Table 3, Cases 1 and 2.

of the energy packets to "zig-zag" lines. Therefore, energy packets emitted from the peripheral zones and directed to the central ones, where dense particle phase exists, may be scattered towards the wall boundaries reducing in that way, the possibility to be absorbed. Under these conditions, the enhancement may turn to reduction of absorption. In order to quantify this phenomenon, the ratio of the total thermal energy absorbed by the gas–particle zones over the total energy emitted by the same zones is calculated and results are presented in Fig. 7. The higher values of the absorption to emission ratio correspond to isotropic scattering. The enhancement of absorption due to scattering is identifiable, since the scattering curves lie above the non-scattering ones for all cases, except for anisotropic scattering, large particles and dilute concentrations where this tendency is reversed, as mentioned earlier.

4. Conclusions

The physically realistic approach for the scattering behaviour of coal combustion particles is the anisotropic, strongly forward scattering. However, there are cases where a simplification is needed to reduce the computational effort. The competing approaches are the isotropic scattering and neglecting of scattering. It was shown that, in realistic conditions, the second approach gives results closer to anisotropic scattering with the exception of large particle loading and fine pulverisation, where both simplifications may lead to significant errors. Therefore, while in atmospheric coal combustion, neglecting of scattering is a reasonable approach, in PPCC conditions the anisotropic scattering of coal combustion particles should be taken into account, especially as the operational pressure level increases.

The P-1 approximation gave results in satisfactory agreement with the Monte Carlo method. This is because in coal-fired furnaces the presence of combustion particles implies sufficiently large optical depth to avoid the known shortcoming of P-1 when applied to optically thin media. This behaviour is favoured in applications where the optical depth is further increased, such as the large scale atmospheric boilers with significantly larger than the examined geometric dimensions, and in PPCC combustors, where the optical depth increases following the particle loading.

It was shown that fly-ashes characterised by refractive indices as low as these measured by Goodwin, are almost conservative scatterers. Completely different is the behaviour of coal and char particles which, under the assumption of isothermal gaseous and particulate phases, almost shaped the wall heat flux near the inlet areas. Because of this opposing behaviour, future measurements of the fly-ash optical properties should restore the wavelength dependence of the refractive index of fly-ashes containing progressively higher percentages of unburned fuel.

Acknowledgements

Part of this work was financially supported by the Commission of the European Union under the JOULE II CT92-153 project "Evaluation of Pressurised Pulverised Coal Combustion with CO_2 recirculation". The first author would also like to acknowledge the Fluid Mechanics Department of the University of Erlangen-Nürnberg for hosting him within the EU-funded TMR CT-98-224 network "Fundamental improvements in radiative heat transfer — RADIARE".

References

[1] R. Viskanta, M.P. Mengüç, Radiation heat transfer in combustion systems, Prog. Energy Combust. Sci 13 (1987) 97–160.
[2] J.R. Howell, The Monte Carlo method in radiative heat transfer, J. Heat Transfer 120 (1998) 547–560.
[3] F.R. Steward, P. Cannon, The calculation of radiative heat flux in a cylindrical furnace using the Monte Carlo method, Int. J. Heat Mass Transfer 14 (1971) 245–262.
[4] H.A.J. Vercammen, G.F. Froment, An improved zone method using Monte Carlo techniques for the simu-

lation of radiation in industrial furnaces, Int. J. Heat Mass Transfer 23 (1980) 329–337.
[5] R.P. Gupta, T.F. Wall, J.S. Truelove, Radiative scatter by flyash in pulverized-coal-fired furnaces: application of the Monte Carlo method to anisotropic scatter, Int. J. Heat Mass Transfer 26 (1983) 1649–1660.
[6] C.V.S. Murty, Evaluation of radiation reception factors in a rotary kiln using a modified Monte Carlo scheme, Int. J. Heat Mass Transfer 36 (1993) 119–133.
[7] P.J. Coelho, J.M. Gonçalves, M.G. Carvalho, D.N. Trivic, Modelling of radiative heat transfer in enclosures with obstacles, Int. J. Heat Mass Transfer 41 (1998) 745–756.
[8] A.C. Ratzel III, J.R. Howell, Two dimensional radiation in absorbing–emitting–scattering media using the P–N approximation, J. Heat Transfer 105 (1983) 333–340.
[9] M.P. Mengüç, R. Viskanta, Radiative transfer in three-dimensional rectangular enclosures containing inhomogeneous, anisotropically scattering media, J. Quant. Spectrosc. Ratiat. Transfer 33 (1985) 533–549.
[10] M.P. Mengüç, R. Viskanta, Radiative transfer in axisymmetric, finite cylindrical enclosures, J. Heat Transfer 108 (1986) 271–276.
[11] N. Selçuk, Evaluation of spherical harmonics approximation for radiative transfer in cylindrical furnaces, Int. J. Heat Mass Transfer 33 (1990) 579–581.
[12] F. Liu, E.S. Garbet, J. Swithenbank, Effects of anisotropic scattering on radiative heat transfer using the P-1 approximation, Int. J. Heat Mass Transfer 35 (1992) 2491–2499.
[13] F. Liu, J. Swithenbank, E.S. Garbet, The boundary condition of the P–N approximation used to solve the radiative transfer equation, Int. J. Heat Mass Transfer 35 (1992) 2043–2052.
[14] M.P. Mengüç, R. Viskanta, A sensitivity analysis for radiative heat transfer in pulverized coal-fired furnaces, in: Proc. 23rd Nat. Heat Trans. Conf., 221-229, Denver, 1988.
[15] A.G. Blokh, Heat Transfer in Steam Boiler Furnaces, Hemisphere, New York, 1988 (Chap. 3).
[16] S.A. Boothroyd, A.R. Jones, A comparison of radiative characteristics for flyash and coal, Int. J. Heat Mass Transfer 29 (1986) 1649–1654.
[17] D.G. Goodwin, M. Mitchner, Flyash radiative properties and effects on radiative heat transfer in coal-fired systems, Int. J. Heat Mass Transfer 32 (1989) 627–638.
[18] K.H. Im, R.K. Ahluwalia, Radiation properties of coal combustion products, Int. J. Heat Mass Transfer 36 (1993) 293–302.
[19] F. Liu, J. Swithenbank, The effects of particle size distribution and refractive index on fly-ash radiative properties using a simplified approach, Int. J. Heat Mass Transfer 36 (1993) 1905–1912.
[20] C.F. Bohren, D.R. Huffman, Absorption and Scattering of Light by Small Particles, Wiley, New York, 1983.
[21] S.A. Boothroyd, A.R. Jones, K.W. Nicholson, R. Wood, Light scattering by flyash and the applicability of Mie theory, Comb. Flame 69 (1987) 235–241.
[22] J.G. Marakis, Application of narrow and wide band models for radiative transfer in planar media, Int. J. Heat Mass Transfer, submitted August 1999.
[23] M.Q. Brewster, T. Kunitomo, The optical constants of coal, char and limestone, J. Heat Transfer 106 (1984) 678–683.
[24] P.R. Solomon, R.M. Carangelo, P.E. Best, J.R. Markham, D.G. Hamblen, The spectral emittance of pulverized coal and char, in: Twenty-first Symp. (Int.) on Combustion, Combustion Institute, Pittsburgh, 1986, pp. 437–446.
[25] J.H. Joseph, W.J. Wiscombe, J.A. Weinman, The Delta-Eddington approximation for radiative heat transfer, J. Atmos. Sci 33 (1976) 2452–2459.
[26] R. Siegel, J.R. Howell, Thermal Radiation Heat Transfer, 3rd ed., Taylor and Francis, Washington, DC, 1992.
[27] M.Q. Brewster, Thermal Radiative Transfer and Properties, Wiley, New York, 1992.
[28] G. Gouesbet, G. Grehan, B. Maheu, Single scattering characteristics of volume elements in coal clouds, Appl. Opt 22 (1983) 2038–2050.
[29] M.P. Heap, T.M. Lowes, R. Walmsley, H. Bartelds, P. Lavaguerese, Further furnace investigations and the evaluation of the radiative heat transfer models, Doc. Nr. F 37/a/4, International Flame Research Foundation, 1977.
[30] H.L. Wu, N. Fricker, An investigation of the behavior of swirling jet flames in a narrow cylindrical furnace, in: 2nd Members' Conf., International Flame Research Foundation, Ijmuiden, Netherlands, 1971.
[31] J.S. Truelove, Evaluation of the De Macro–Locwood flux model for radiative heat transfer in an axisymmetric cylindrical geometry, AERE—R 9158, AERE Harwell, Oxfordshire, UK, 1978.
[32] W.A. Fiveland, A discrete ordinates method for predicting radiative heat transfer in axisymmetric enclosures, ASME Paper No. 82-HT-20, 1982.
[33] D. Dunn-Rankin, A.R. Kerstein, Influence of ash on particle size distribution evolution during coal combustion, Comb. Flame 74 (1988) 207–218.